circNRIP1 facilitates keloid progression via FXR1-mediated upregulation of miR-503-3p and miR-503-5p

BAOLIN WANG[1], HANG YIN[2], HONGMEI ZHANG[3] and TIANTIAN WANG[1]

Departments of [1]Dermatology, [2]Neurosurgery and [3]Pharmacy,
Zaozhuang Municipal Hospital, Zaozhuang, Shandong 277100, P.R. China

Received June 16, 2020; Accepted January 25, 2021

DOI: 10.3892/ijmm.2021.4903

Abstract. Circular nuclear receptor interacting protein 1 (circNRIP1) is implicated in tumor initiation and progression; however, the underlying mechanism of keloid progression is unclear. To the best of our knowledge, the present study is the first to characterize the contribution of circNRIP1 to keloid progression and evaluate the potential underlying molecular mechanisms using keloid-derived fibroblasts. The expression profile of circNRIP1 was confirmed in keloid tissue. The contribution of circNRIP1 to keloid progression was investigated via loss-of-function assays. Furthermore, the molecular mechanism by which circNRIP1 contributes to pre-microRNA (miR)-503 maturation through blocking Fbxo4-mediated Fragile-X mental retardation 1 (FXR1) ubiquitination was verified. Finally, the biological functions of FXR1, miR-503-3p, and miR-503-5p in keloid-derived fibroblast proliferation, apoptosis and extracellular matrix accumulation were confirmed. circNRIP1 was highly expressed in keloid tissue and keloid-derived fibroblasts. Functional analysis showed that circNRIP1 knockdown successfully blocked the proliferation and expression of extracellular matrix-associated proteins while increasing the rate of apoptosis in keloid-derived fibroblasts. Mechanistically, circNRIP1 maintained FXR1 stability by impeding Fbxo4-mediated FXR1 ubiquitination and degradation. Additionally, FXR1 increased the abundance of miR-503-3p and miR-503-5p by contributing to pre-miR-503 maturation. Knockdown of FXR1, miR-503-3p and miR-503-5p also inhibited proliferation and extracellular matrix accumulation in keloid-derived fibroblasts and increased levels of cell apoptosis. Collectively, the present study confirmed that circNRIP1 contributed to pre-miR-503 maturation via blocking Fbxo4-mediated FXR1 ubiquitination and degradation, which facilitates keloid progression. These results indicate that circNRIP1 has potential as a novel therapeutic target for the control and/or treatment of keloids.

Correspondence to: Dr Tiantian Wang, Department of Dermatology, Zaozhuang Municipal Hospital, 41 Longtou Middle Road, Shizhong, Zaozhuang, Shandong 277100, P.R. China
E-mail: titiwangsd@163.com

Key words: keloid, circular nuclear receptor interacting protein 1, Fragile-X mental retardation 1, microRNA-503-3p, microRNA-503-5p

Introduction

Keloids are benign fibroproliferative tumors that commonly occur in response to tissue injury. These pathological scars are characterized by hyperproliferation of fibroblasts and abnormal deposition of collagen fibers (1,2). Although keloids are benign hyperplasias, they induce esthetic deformity and dermatological dysfunction by invading adjacent normal tissue (3,4). In addition, frequent keloid-associated episodes of pain and itching also result in psychological and physical distress. No satisfactory treatment strategy has been developed, primarily because of the high recurrence rate of keloids, which can reach up to 70-80% post-excision (5,6). Extensive research has indicated that keloid development is complex and involves alterations in non-coding RNAs, DNA methylation and histone modification (7-9); however, the precise pathological mechanisms underlying how keloid formation and progression are initiated and regulated remain unknown, which has hindered the development of novel therapeutic strategies.

Accumulating evidence has indicated that circular (circ) RNAs produced from precursor mRNA backsplicing are aberrantly expressed in multiple diseases and are associated with cell proliferation, apoptosis and metastasis (10,11). For example, circ-low density lipoprotein receptor class A domain containing 3, a well-characterized circRNA, regulates the proliferation, migration and invasion of pancreatic cancer cells via the microRNA (miRNA or miR)-137-3p/PTEN axis (12). Additionally, circ-collagen type III α 1 chain-859267 has been shown to regulate the expression levels of type I collagen by sponging miR-29c in human dermal fibroblasts (13). Shi *et al* (14) investigated circRNA expression profiles in keloids via microarray analysis and found that a number were abnormally expressed, including 24 that were significantly downregulated and 52 markedly upregulated in keloids compared with normal skin tissue. Therefore, it was hypothesized that circRNAs may be involved in the regulation of keloid progression. circ-nuclear receptor interacting protein 1 (NRIP1) originates from the *NRIP1* gene located on chromosome 21 and is the product of the head-to-tail splicing of exons 2 and 3 (15). Several

studies have investigated the expression profile and function of circNRIP1 in various types of cancer (16,17). One study (15) showed that circNRIP1 promotes the proliferation, migration and invasion of gastric cancer cells via the AKT1/mTOR pathway, while another study (18) reported that silencing of circNRIP1 inhibits proliferation and induces apoptosis in breast cancer. Although the contribution of circNRIP1 to tumor growth and metastasis has been widely reported (16,17), pronounced knowledge gaps remain regarding the biology of keloid progression. Recent studies have shown that dysregulation of circRNAs can affect gene expression profiles by creating complex regulatory networks through interactions with proteins and RNA (19-21). Du *et al* (22) revealed that circ-Foxo3 promotes mouse double minute 2 homolog-induced p53 ubiquitination and degradation, causing an overall decrease in the levels of p53. circβ-catenin stabilizes β-catenin by impeding GSK3β-mediated β-catenin phosphorylation and degradation, leading to activation of the Wnt pathway (23). It was hypothesized that circNRIP1 may harbor a putative binding site for the RNA-binding protein Fragile-X mental retardation 1 (FXR1) and that circNRIP1 may be involved in keloid progression via regulating FXR1.

The aim of the present study was to investigate the putative role of circNRIP1 in keloid progression and the underlying regulatory mechanisms by performing loss-of-function, RNA pulldown and RNA immunoprecipitation assays to provide novel insight into keloid progression and potential therapeutic options.

Materials and methods

Patient tissue samples. Between January 2016 and August 2018, 50 keloid and 50 matched normal skin tissue samples were obtained from 50 patients (21 males and 29 females) in Zaozhuang Municipal Hospital (Zaozhuang, China). Diagnosis of hypertrophic scar was confirmed via routine pathological examination with clinical symptoms such as pain, growth, hyperemia and pruritus. Following excision of keloid tissues at the Department of Plastic Surgery, skin samples were immediately stored in liquid nitrogen for further processing. A total of 50 patients was enrolled (age, 31.86±6.37 years) who exhibited non-pedunculated keloid on the chest (n=18), back (n=17) and upper arm (n=15) for ≥1 year. The etiology of hypertrophic scarring included acne (n=18), blister (n=13), post-operative (n=14) and unknown (n=5). Furthermore, none of the patients had received systemic and topical therapy for >60 days before pathological examination. The present study was approved by the Clinical Research Ethics Committee of Zaozhuang Municipal Hospital. Additionally, written informed consent was obtained from all patients.

Cell culture. Primary cultures of keloid-derived fibroblasts and normal dermal fibroblasts were established as previously described (2). Briefly, keloid and matched normal skin tissue were excised and dissected into 1-mm3 pieces. Subsequently, the pieces were digested with 0.25% trypsin at 37˚C for 3 min. After washing and mechanical dissociation, the fibroblasts were filtered, centrifuged (500 x g for 5 min at 25˚C) and resuspended in DMEM supplemented with 10% fetal bovine serum (both Thermo Fisher Scientific, Inc.) at 37˚C in a tissue culture incubator with 5% CO_2. The medium was changed every 3 days. Fibroblasts from generation 2 to 5 were used in subsequent experiments.

RNA extraction and reverse transcription-quantitative (RT-q) PCR. Total RNA from fibroblasts and tissue was extracted using the RNAeasy Gamma Animal RNA Extraction kit (Beyotime Institute of Biotechnology). Following RNase-R treatment, the M-MLV universal RT-PCR kit (Beijing Solarbio Science & Technology Co., Ltd.) was used for cDNA synthesis, according to the manufacturer's instructions. The expression levels of circRNAs and miRNAs was evaluated by qPCR using the SuperScript IV RT-PCR kit (Thermo Fisher Scientific, Inc.). The reaction conditions for PCR (5 μl cDNA) were as follows: 95˚C for 10 min, followed by 40 cycles of 93˚C for 15 sec and 54˚C for 60 sec. *GAPDH* and *U6* were used as controls for circRNA and miRNA, respectively. The $2^{-\Delta\Delta Cq}$ method was employed to calculate relative circRNA and miRNA levels (24). The primers were designed and synthesized by Sangon Biotech Co., Ltd. The primer sequences were as follows: circNRIP1, forward, 5'-AGTTGCTCC AATGACAGA GTTACC-3' and reverse, 5'-CCTCCTTCA GTCAAGTGT GCATC-3'; pre-miR-503, forward, 5'-TGCCCTAGCAGCGGG AAC-3' and reverse, 5'-ACCCTGGCA GCGGAAACAATA-3'; miR-503-3p, forward, 5'-GGGGTATTGTTTCCGCTGCCA GG-3', reverse, 5'-CCTGGC AGCGGAAACAATACCCC-3' and RT, 5'-GTCGTA TCCAGTGC AG GGTCCGAGGTATTC GCACTGGATACGACCCTGGC-3'; miR-503-5p, forward, 5'-CGTAGCAGCGGGAACAGTT-3', reverse, 5'-AGTGCA GGGTCCGAGGTATT-3' and RT, 5'-GTCGTATCCAGTGCA GGGTCCGAGGTATTCGCACTGGATACGACCTGCAG-3'; GAPDH, forward, 5'-GTCAACGGATTTGGTCGTATT G-3' and reverse, 5'-CCGTTCTCAGCCATGTAGTT-3'; and U6, forward, 5'-TCGGCAGCACATATACTA AAAT-3', reverse, 5'-CGCTTCACGAATTTGCGTGTCAT-3' and RT, 5'-CGC TTCACGAATTTGCGT GTCAT-3'.

Cell transfection. Keloid-derived fibroblasts ($1x10^5$ per well) were seeded in a 6-well plate and grown overnight at 37˚C. Small interfering (si)RNA targeting *NRIP1* or *FXR1* was cloned into the pENTR H1 vector. Plasmid vectors (pcDNA-circNRIP1: siNRIP1#1, siNRIP1#2; pcDNA-FXR1: siFXR1#1, siFXR1#2) were designed and synthesized by Sangon Biotech Co., Ltd. A mock vector with no siRNA sequence was used as a control. miR-503 precursor pGCMV vectors were provided by Shanghai GenePharma Co., Ltd. Front and back circular frames were synthesized by Sangon Biotech Co., Ltd. and inserted into the pcDNA3.1 (+) circRNA mini vector for transcript circularization. The expression vectors for Flag-tagged MS2 coat protein were provided by Weizhen Biotech Co., Ltd. Flag-tagged expression vectors for full-length Fbxo4 and HA-tagged expression vectors for full-length FXR1 were provided by Weizhen Biotechnology. Keloid-derived fibroblasts were transfected with the corresponding plasmids (25 nM) for 2 days at 37˚C using Lipofectamine® 3000 (Thermo Fisher Scientific, Inc.) according to the manufacturer's protocol. Overexpression and knockdown efficiency were monitored by RT-qPCR and western blotting after transfection for 24 h. The targeted sequences were as follows: siNRIP1#1,

5'-GACAGACGGAAGTGTTTGGAT-3'; siNRIP1#2, 5'-GAA TCTGAAGACTCCGGA T-3'; siFXR1#1, 5'-GGCAAAGTG ATCGGAAAGA-3' and siFXR1#2, 5'-CGAGCTGAGTGA TTGGTCA-3'. The inhibitor sequences were as follows: miR-503-3p, 5'-CCTGGCAGCGGAAACAAT ACCCC-3'; miR-503-5p, 5'-CTGCAGAACTGTTCCCGCTGCTA-3' and control (ctrl), 5'-TGACTGTACTGACTCGACTG-3'.

Cell proliferation and colony formation assay. For the Cell Counting Kit (CCK)-8 assay, keloid-derived fibroblasts (3,000 per well) were plated in 96-well plates. Following incubation for different durations (1, 2 and 3 days), cell viability was determined by adding 10 μl CCK-8 reagent to each well, according to the manufacturer's instructions (Abmole Bioscience, Inc.). The absorbance (450 nm) was determined using a microplate reader (Shenzhen Mindray Bio-Medical Electronics Co., Ltd.). For the colony formation assay, keloid-derived fibroblasts (3,000 per well) were plated in 6-well plates. After incubation at 37˚C for two weeks, keloid-derived fibroblasts were fixed in 4% paraformaldehyde for 20 min at 25˚C and then stained with 0.1% crystal violet (Beyotime Institute of Biotechnology) for 20 min at 25˚C. Visible colonies were observed using a WMS-1033 Digital light biomicroscope at 200x magnification (Shanghai Wumox Optical Instrument Co., Ltd.). Images were captured using an EOS M50 digital camera (Canon, Inc.) and quantified by three observers.

Flow cytometric assays. For cell apoptosis, keloid-derived fibroblasts underwent double staining with 20 ng/l FITC-Annexin V (10 μl, 30 min, 25˚C) then 50 ng/l propidium iodide (5 μl, 5 min, 25˚C) using the Annexin V-FITC cell apoptosis detection kit (Beyotime Institute of Biotechnology) according to the manufacturer's instructions. Cell apoptosis was analyzed using a BD FACSCelesta flow cytometer (BD Biosciences). For cell cycle analysis, keloid-derived fibroblasts were stained with propidium iodide using the DNA Content Quantitation Assay kit (Beijing Solarbio Science & Technology Co., Ltd.) following the manufacturer's protocol and then analyzed by flow cytometry. The percentage of fibroblasts in the G_0/G1, S and G_2/M phases were counted using FlowJo10.4 software (Becton, Dickinson & Company).

Western blot analysis. Total protein from fibroblasts and tissue was extracted on ice using the Total Extraction Sample kit (Sigma-Aldrich; Merck KGaA). The protein concentration was determined via BCA assay (Beyotime Institute of Biotechnology). 50 μg protein were separated by 12 or 8% SDS-PAGE and then electrophoretically transferred onto PVDF membranes. Following incubation with 5% non-fat milk for 2 h at 25˚C, the membranes were incubated with rabbit anti-FXR1 (1:1,000; cat. no. ab155124), mouse anti-fibronectin (1:500; cat. no. ab6328), anti-collagen I (1:1,000; cat. no. ab6308), anti-collagen III (1:1,000; cat. no. ab6310), rabbit anti-SMN/Gemin 1 (1,1000; cat. no. ab108531), anti-FBXO4 (1:2,000; cat. no. ab153803) and mouse anti-β actin antibody (1:25,000; cat. no. ab49900; all Abcam) for 12 h at 4˚C and then with horseradish peroxidase-conjugated goat anti-rabbit or anti-mouse IgG H&L secondary antibody (both 1:20,000; cat. nos. ab205718 and ab6789, respectively; both Abcam) for 2 h at 25˚C. Protein bands were visualized using Cobas E 601electrochemiluminescence (Roche Diagnostics) and X-ray film. ImageJ 2.1 software (National Institutes of Health) was used for densitometric analysis. GAPDH (1:10,000; cat. no. ab181602; Abcam) was used as an internal control.

Database analysis. The targets of circNRIP1 were acquired using the RNA Interactome Database (rna-society.org/rnainter/home.html). The binding sites of FXR1 om miR-503 were acquired through starBase (starbase.sysu.edu.cn/).

RNA pulldown and RNA immunoprecipitation assay (RIPA). For the RNA pulldown assay, a biotin-labeled RNA probe complementary to circNRIP1 was designed and synthesized by Sangon Biotech Co., Ltd. Then, 293T cells ($1x10^7$) and keloid-derived fibroblasts were harvested, washed with ice-cold PBS, lysed with RIPA Lysis Buffer (500 μl, Beyotime Institute of Biotechnology) and incubated with biotinylated probes (3 μg) for 2 h at 25˚C. Streptavidin C1 magnetic beads (50 μl; Thermo Fisher Scientific, Inc.) were added to each binding reaction followed by incubation at room temperature for 60 min. After briefly washing the beads with co-IP buffer, the bound proteins were detected using western blotting as aforementioned. For RIPA, $1x10^7$ 293T cells or keloid-derived fibroblasts were harvested, washed with ice-cold PBS, lysed with RIPA Lysis Buffer (500 μl; Beyotime Institute of Biotechnology) and isolated using the RNAeasy Gamma Animal RNA Extraction kit (TransGen Biotech Co., Ltd.). The cells were incubated with 5 μg primary antibody from Abcam [anti-FXR1 (1:1,000; cat. no. ab155124), anti-Dicer (1:1,000; cat. no. ab227518), anti-GAPDH (1:10,000; cat. no. ab181602; Abcam); anti-Flag (1:1,000; cat. no. ab236777)] for 2 h at 4˚C. Subsequently, each sample was supplemented with 50% protein A-Sepharose slurry (50 μl) and incubated for 4 h at 4˚C. Following centrifugation (1,000 x g, 4˚C for 3 min) and three PBS washes, samples were resuspended in 0.5 ml Tris reagent (Sigma-Aldrich; Merck KGaA) followed by elution. The eluted, co-precipitated RNA was subjected to RT-qPCR as aforementioned to measure the levels of the circRNA of interest. Telomerase RNA component (TERC) was used as the positive control.

Co-immunoprecipitation (CO-IP) assay. Cell lysate was produced using RIPA Lysis Buffer (Beyotime Institute of Biotechnology) and supernatant were collected. A total of 200 μl A/G beads (Thermo Fisher Scientific, Inc.) were washed with pre-cooled PBS. Then, 2 μg antibody from Abcam [anti-Flag (1:30; cat. no. ab236777), anti-HA (1:30; cat. no. ab236632)] was added, followed by incubation for 3 h at 4˚C. Following centrifugation (4,000 x g, 4˚C, 60 sec) and washing (3 times), preprepared cell extracts (1 ml) were added and incubated overnight at 4˚C in the presence of phenylmethylsulfonyl fluoride (0.5 mM) and protease inhibitors (10 μl). Following centrifugation (4,000 x g, 4˚C, 60 sec) and washing (3 times) with bead wash solution, the precipitates were boiled in loading buffer (60 μl) and incubated for 300-600 sec (100˚C). Western blot analysis was conducted as aforementioned to evaluate the co-IP results.

Northern blot assay. Northern blotting was conducted using a High Sensitive miRNA Northern Blot Assay kit according

to the manufacturer's instructions (Signosis, Inc.). Total RNA (10 μg) was denatured with glyoxal loading dye at 50˚C for 30 min, loaded onto agarose gels (1.2%) and electrophoresed for 150 min at 60 V. RNA was transferred by capillarity onto a Hybond N+ membrane (GE Healthcare) overnight in 10X saline sodium citrate buffer at 4˚C. After crosslinking using UV light (1,200 x 100 mJ/cm^2), the membrane was washed with Tris for 20 min. Subsequently, prehybridization (62˚C, 2 h) and hybridization (62˚C, 16 h) were performed in Northern Max buffer (Sigma-Aldrich; Merck KGaA). After washing, the blots were visualized using two-color infrared laser imaging (Gene Company, Ltd.). Then bands were analyzed by ImageJ 1.8 software (National Institutes of Health).

Statistical analysis. All statistical analysis was performed using GraphPad Prism v.8 (GraphPad Software, Inc.). All data are presented as the mean ± SEM of three independent repeats. Paired Student's t-test was used to compare differences between two groups. Significance between multiple groups was analyzed by one-way ANOVA followed by Tukey's post hoc test. Correlations were analyzed via Pearson's correlation analysis. $P<0.05$ and $P<0.01$ were considered to indicate a statistically significant difference.

Results

circNRIP1 is overexpressed in human keloid tissue. In order to identify whether circNRIP1 is expressed in human keloid tissue, 50 keloid and adjacent normal skin tissue samples were collected. RT-qPCR showed that the levels of circNRIP1 in keloid tissue were 3.24-fold higher than those of adjacent normal skin tissue (Fig. 1A). Furthermore, the expression levels of circNRIP1 in keloid-derived and human normal fibroblasts were compared. circNRIP1 expression was significantly increased in keloid-derived fibroblasts compared with that in normal human fibroblasts (Fig. 1B).

circNRIP1 knockdown suppresses proliferation and extracellular matrix accumulation but promotes cell apoptosis in keloid-derived fibroblasts. In order to confirm whether circNRIP1 participates in the regulation of cell proliferation and apoptosis in fibroblasts, expression of circNRIP1 was knocked down using siRNA (Fig. 1C). Cell viability curves constructed at different time points using CCK-8 assay revealed that siRNA-mediated silencing of circNRIP1 significantly inhibited cell viability compared with the control (Fig. 1D). In addition, colony formation assay demonstrated that cell survival was significantly decreased following inhibition of circNRIP1 (Fig. 1E and F). Subsequently, flow cytometric analysis was used to evaluate whether circNRIP1 influenced the proliferative ability of keloid-derived fibroblasts via effects on cell apoptosis and cycle progression. The rate of apoptosis was significantly higher in circNRIP1-silenced keloid-derived fibroblasts than in control cells (Fig. 1G and H). Additionally, circNRIP1 knockdown resulted in a marked increase in the G_0/G_1 phase and decrease in the S phase of the cell cycle compared with control fibroblasts (Fig. 1I and J). In order to assess whether circNRIP1 has a role in extracellular matrix deposition, the accumulation of extracellular matrix components was assessed by western blotting. Expression of fibronectin, α-smooth muscle actin (SMA), collagen I and III was decreased in circNRIP1-silenced fibroblasts compared with that in control fibroblasts (Fig. 1K and L). Collectively, these results indicated that circNRIP1 facilitated keloid progression.

circNRIP1 stabilizes FXR1 by impeding Fbxo4-mediated FXR1 ubiquitination. Next, the mechanism by which circNRIP1 facilitates keloid-derived fibroblast proliferation and suppresses apoptosis was investigated. Using the bioinformatic database RNAInter, 21 putative downstream targets of circNRIP1 were identified (Fig. 2A). Among these downstream targets, members of the fragile X protein family (FXR1, FXR2 and FMR1) were identified as binding partners. RNA binding protein FXR1 (score, 0.6116) is of particular interest due to the high score and FXR1 biological function. The binding sites in FXR1 and circNRIP1 are shown in Fig. 2B and C, respectively. Subsequently, the expression profile of FXR1 in keloid tissue was assessed. Expression levels of FXR1 in keloid tissue were 2.38-fold higher than in adjacent normal skin tissue (Fig. 2D and E). Moreover, FXR1 expression was also higher in keloid-derived fibroblasts relative to normal human fibroblasts (Fig. 2F), suggesting that FXR1 ws positively associated with circNRIP1 expression in keloids. Furthermore, knockdown of circNRIP1 led to a significant decrease in expression of FXR1 (Fig. 2G and H). Pearson's correlation analysis also confirmed that circNRIP1 levels were positively associated with the expression of FXR1 in keloid tissues (Fig. 2I). These results suggested that circNRIP1 was involved in maintaining FXR1 stability.

RNA pulldown assays were used to investigate the regulatory mechanism involved in circNRIP1-mediated maintenance of FXR1 stability. The results showed that circNRIP1 was pulled down with endogenous FXR1 protein, but not with GAPDH (negative control; Fig. 2J). RNA pull-down assays using 293T cells transfected with Flag-FXR1 and circNRIP1-MS2 or its antisense variant demonstrated that circNRIP1 was pulled down with Flag-FXR1, but not Flag-GAPDH (Fig. 2K). RIPA was performed to validate the interaction between circNRIP1 and FXR1. Compared with the positive control (TERC), circNRIP1 was enriched in FXR1 binding (Fig. 2L). These results confirmed that circNRIP1 specifically interacted with the RNA-binding protein FXR1 in keloid-derived fibroblasts.

In order to clarify how circNRIP1 regulates FXR1 stability, circNRIP1-depleted keloid-derived fibroblasts were treated with proteasome inhibitor MG132. FXR1 expression was significantly increased following circNRIP1 depletion in the presence of MG132 compared with circNRIP1 depletion-alone (Fig. 3A and B). This suggested that the role of circNRIP1 in maintaining FXR1 stability was associated with proteasomal degradation. Knockdown of endogenous circNRIP1 in fibroblasts notably enhanced the levels of endogenous FXR1 ubiquitination (Fig. 3C), whereas FXR1 ubiquitination was markedly diminished by circNRIP1 overexpression in 293T cells (Fig. 3D). Combined, these data indicated that circNRIP1 stabilized FXR1 protein by impeding its ubiquitination and proteasomal degradation in keloid-derived fibroblasts. Subsequently, E3 ubiquitin ligase Fbxo4 was overexpressed, which led to a significant increase in the expression levels of Fbxo4 (Fig. 3E and F). Moreover, circNRIP1 overexpression

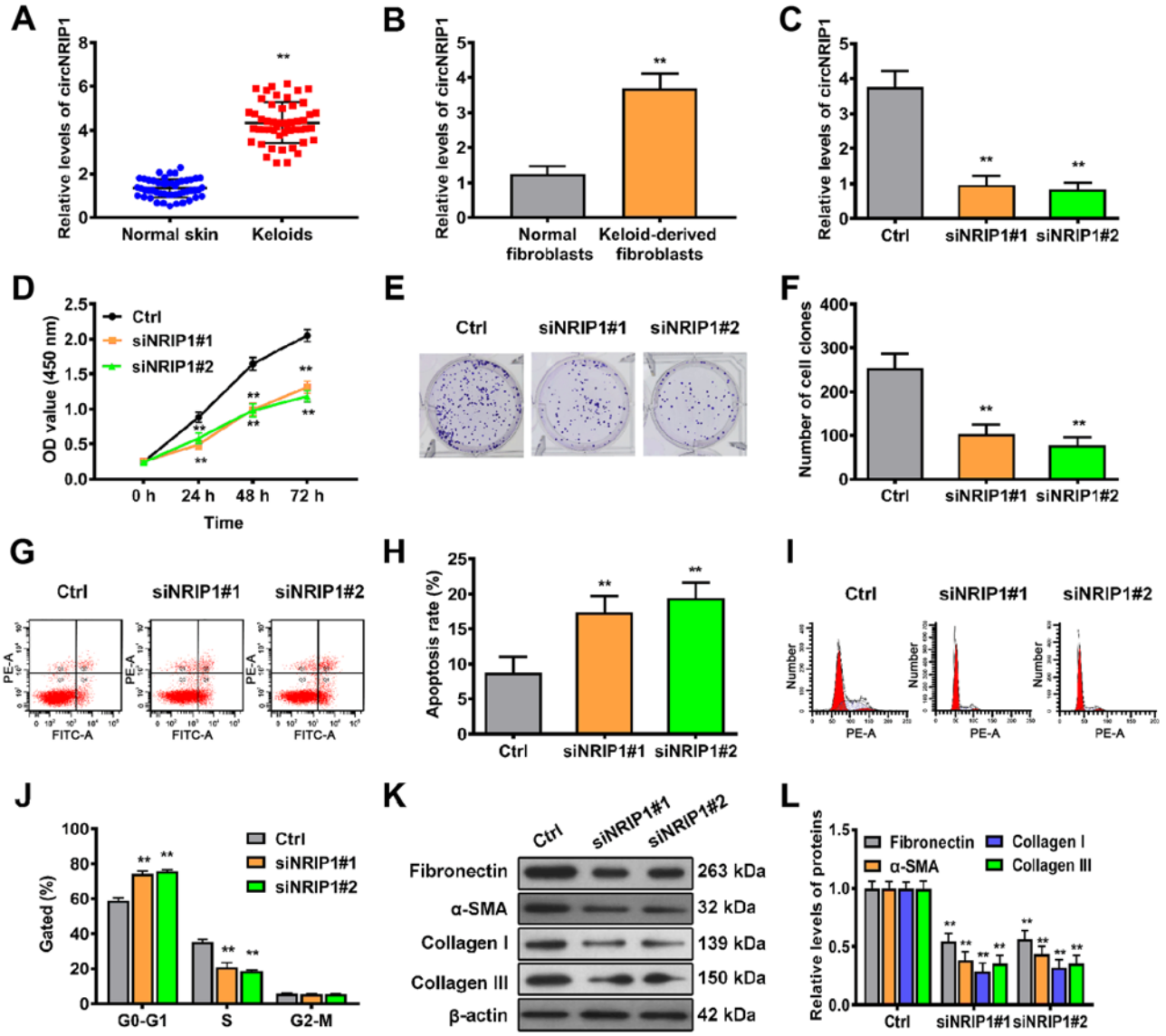

Figure 1. circNRIP1 is upregulated in keloid tissue and is associated with keloid progression. RT-qPCR assay was performed to detect the abundance of circNRIP1 in (A) keloid and adjacent normal skin tissue and (B) keloid-derived and normal human fibroblasts. (C) Knockdown efficiency of circNRIP1 was evaluated in keloid-derived fibroblasts by RT-qPCR. (D) Cell Counting Kit-8 assay was used to determine the viability of keloid-derived fibroblasts in the presence or absence circNRIP1 knockdown. Colony-forming ability of keloid-derived fibroblasts was (E) assessed and (F) quantified. Flow cytometric assays were conducted to evaluate the effect of circNRIP1 on (G and H) apoptosis and (I and J) cell cycle progression of keloid-derived fibroblasts. (K and L) Changes in the expression of extracellular matrix-associated regulatory proteins in keloid-derived fibroblasts were determined by western blot assay. **P<0.01 vs. Ctrl or human normal fibroblasts. circNRIP1, circular nuclear receptor interacting protein 1; RT-q, reverse transcription-quantitative; Ctrl, control; si, small interfering; OD, optical density.

rescued Fbxo4-induced FXR1 degradation (Fig. 3E and G). circNRIP1 overexpression also inhibited the interaction between FXR1 and Fbxo4: FXR1 co-immunoprecipitated with less Fbxo4, while Fbxo4 also co-immunoprecipitated with less FXR1 (Fig. 3H and I). These results collectively demonstrated that circNRIP1 blocked Fbxo4-mediated FXR1 ubiquitination by inhibiting the interaction between FXR1 and Fbxo4, thereby preventing FXR1 proteasomal degradation.

FXR1 drives keloid-derived fibroblast proliferation and accumulation of extracellular matrix but inhibits apoptosis. In order to evaluate whether FXR1 is functionally involved in keloid progression, FXR1 expression was knocked down in keloid-derived fibroblasts by siRNA transfection (Fig. 4A and B). Silencing FXR1 by transfection of siRNA#1 and siRNA#2 significantly decreased cell viability over 3 days (Fig. 4C). Consistent with the cell viability data, FXR1 knockdown by either of the two siRNAs also significantly decreased the colony-forming ability of fibroblasts (Fig. 4D and E). Next, the effect of FXR1 on cell apoptosis and cell cycle progression in keloid-derived fibroblasts was assessed. The results of flow cytometry showed that silencing FXR1 by siRNA#1 or siRNA#2 transfection significantly increased the rate of apoptosis of keloid-derived fibroblasts compared with control cells (Fig. 4F and G). Additionally, there was a significant increase in the number of FXR1-silenced fibroblasts arrested at the G_1/G_0 phase compared with that in control cells (Fig. 4H and I). Expression levels of extracellular matrix components were detected by western blot assay. Silencing FXR1 significantly decreased the expression levels of fibronectin, α-SMA,

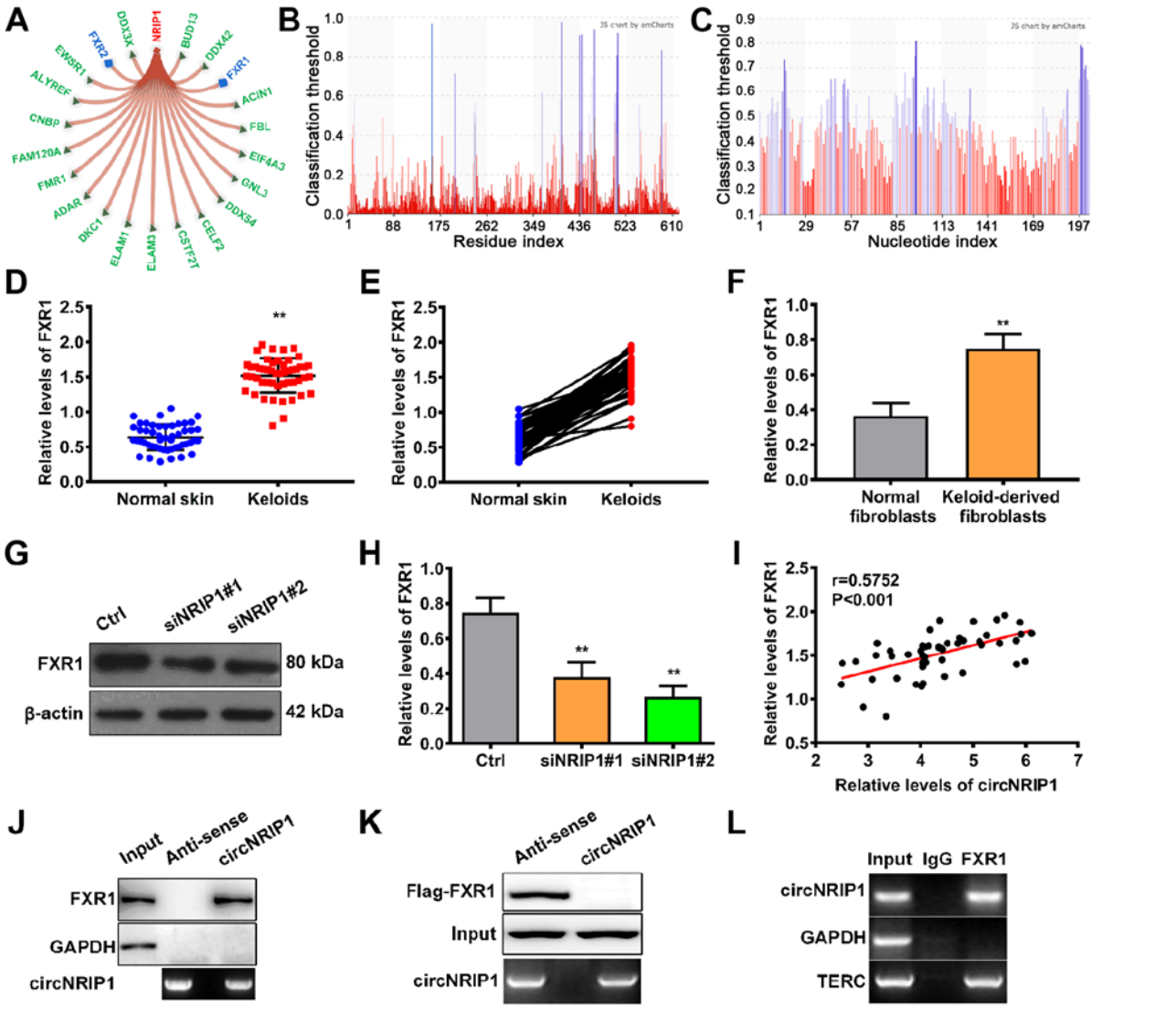

Figure 2. circNRIP1 interacts with FXR1 to maintain its stability. (A) Downstream targets of circNRIP1 were predicted using the RNAInter website. Bioinformatic (PRIdictor) prediction of binding sites within (B) circNRIP1 and (C) FXR1. (D) FXR1 expression levels in keloid and adjacent normal skin tissue were measured by western blot analysis. (E) Association between FXR1 levels in keloid and adjacent normal skin tissue was determined. (F) FXR1 expression levels in keloid-derived and human normal fibroblasts were detected by western blot assay. (G and H) FXR1 expression levels in keloid-derived fibroblasts in the presence or absence of circNRIP1 knockdown were evaluated by western blot assay. (I) Association between circNRIP1 levels and FXR1 expression in keloid tissue was evaluated by Pearson's correlation analysis. (J) Whole-cell lysate from keloid-derived fibroblasts was used for RNA pulldown with biotinylated circNRIP1 or antisense transcripts, followed by western blotting analysis for FXR1. GAPDH was used as a control. (K) Immunoprecipitation of circNRIP1 was performed in whole-cell lysate of 293T cells followed by immunoblotting for FXR1 to assess the interaction between circNRIP1 and FXR1. (L) Keloid-derived fibroblast lysate was subjected to RNA immunoprecipitation assay using anti-FXR1 or anti-IgG followed by reverse transcription-quantitative PCR. GAPDH and TERC mRNA were used as negative and positive controls, respectively. **P<0.01 vs. Ctrl or human normal fibroblasts. circNRIP1, circular nuclear receptor interacting protein 1; FXR1, Fbxo4-mediated FMR1 autosomal homolog 1; TERC, telomerase RNA component; Ctrl, control; si, small interfering.

collagen I and III in circNRIP1-silenced fibroblasts compared with control fibroblasts (Fig. 4J and K). These data revealed that FXR1 served a vital role in keloid progression.

FXR1 modulates the maturation of pre-miR-503. In order to elucidate the mechanism by which FXR1 regulates keloid progression, the potential interacting sites between FXR1 and miRNAs were predicted using starBase. miR-503 of 82 predicted miRNAs were identified; binding sites in pre-miR-503 are shown in Fig. 5A. RT-qPCR was performed to determine the levels of pre-miR-503 in keloid and adjacent normal skin tissue. Levels of pre-miR-503 were significantly decreased in keloid compared with adjacent normal skin tissue (Fig. 5B and C). Similar results were obtained in keloid-derived fibroblasts (Fig. 5D). Moreover, the levels of pre-miR-503 were significantly upregulated following knockdown of FXR1 using either siRNA#1 or siRNA#2 (Fig. 5E). Subsequently, the expression profiles of mature miR-503, miR-503-3p and miR-503-5p were investigated. The levels of miR-503-3p and miR-503-5p were significantly increased in keloid-derived fibroblasts (Fig. 5F and G). However, silencing of FXR1 significantly decreased levels of miR-503-3p and miR-503-5p (Fig. 5H and I). These results indicated that FXR1 contributed to the maturation of miR-503.

In order to confirm this possibility, the interaction between FXR1 and pre-miR-503 was assessed. RNA pulldown assays demonstrated that pre-miR-503 specifically pulled down

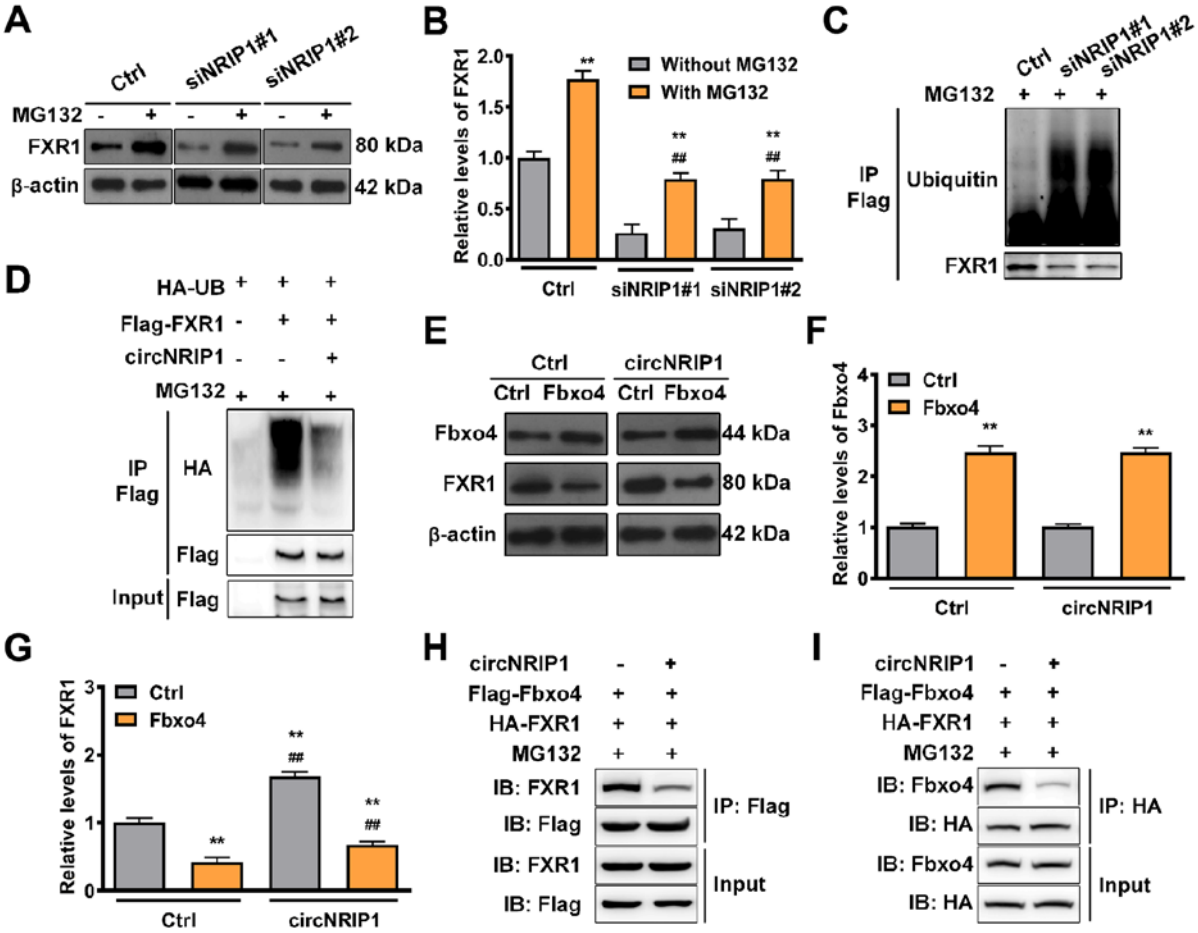

Figure 3. circNRIP1 protects FXR1 from Fbxo4-mediated ubiquitination. (A and B) Expression of FXR1 in keloid-derived fibroblasts in response to MG132 exposure (20 μmol/l) for 6 h was examined by western blot assay. (C) Keloid-derived fibroblasts with circNRIP1 knockdown were immunoprecipitated with anti-Flag antibody and immunoblotted with an anti-HA-ubiquitin antibody following MG132 exposure for 6 h. (D) 293T cells were transfected with HA-UB, Flag-FXR1, or circNRIP1. Whole-cell lysates were immunoprecipitated with the anti-Flag antibody and then immunoblotted with anti-HA-ubiquitin antibody to detect the interaction between FXR1 and Ubiquitin following MG132 exposure (20 μmol/l). (E) Expression of (F) Fbxo4 and (G) FXR1 in keloid-derived fibroblasts transfected with Fbxo4 was investigated by western blot analysis following circNRIP1 overexpression. 293T cells were transfected with Flag-Fbxo4, HA-FXR1 and circNRIP1, followed by MG132 treatment (20 μmol/l, 6 h); cell lysates were immunoprecipitated with (H) anti-Flag or (I) anti-HA antibody. The precipitates and inputs were analyzed by western blot analysis. **P<0.01 vs. Ctrl or MG132 treatment group. $^{\#\#}$P<0.01 vs. MG132 treatment or Fbox4 overexpression group. circNRIP1, circular nuclear receptor interacting protein 1; FXR1, Fbxo4-mediated FMR1 autosomal homolog 1; Ctrl, control; si, small interfering; IP, immunoprecipitation; IB, immunoblot.

with endogenous FXR1 protein but not the negative control GAPDH (Fig. 5J). Consistent with this, pre-miR-503 was able to pull down Flag-FXR1 in 293T cells (Fig. 5K). The interaction between pre-miR-503 and FXR1 was also validated by RIPA, in which pre-miR-503 was enriched for FXR1 binding (Fig. 5L). Furthermore, FXR1 formed complexes with Dicer, a double-stranded RNA nuclease essential for the biogenesis of numerous miRNAs, such as miRNA-103 (25) (Fig. 5M). In order to demonstrate a direct role for FXR1 in pre-miR-503 processing, northern blot analysis was performed using 293T cells transfected with both siFXR1 and pre-miR-503. Upregulation of Flag-tagged FXR1 in 293T cells increased the level of mature miR-503 (Fig. 5N); however, processing of pre-miR-503 into mature miR-503 was impaired in the absence of FXR1 (Fig. 5O). Together, these results demonstrated that FXR1 increased the levels of mature miR-503 via regulating the processing of pre-miR-503.

Mature miR-503 promotes keloid-derived fibroblast proliferation and accumulation of extracellular matrix but inhibits apoptosis. Next, the biological functions of miR-503-3p and miR-503-5p in keloid progression were investigated through loss-of-function experiments. miR-503-3p or miR-503-5p-specific inhibitors were infected into keloid-derived fibroblasts, resulting in knockdown of miR-503-3p or miR-503-5p (Fig. 6A). CCK-8 assay showed that cell proliferation was suppressed by miR-503-3p or miR-503-5p knockdown at different times (Fig. 6B and C), while colony formation assay revealed that knockdown of miR-503-3p or miR-503-5p significantly inhibited the proliferative ability of keloid-derived fibroblasts (Fig. 6D and E). Cell cycle progression and apoptosis were also investigated via flow cytometry following miR-503-3p or miR-503-5p knockdown. Annexin V/PI double staining showed that the rates of apoptosis were significantly higher in fibroblasts in the inhibitor group compared with the control group (Fig. 6F and G). Additionally, cell cycle analysis demonstrated that more fibroblasts were distributed in the G_0/G_1 phase (Fig. 6H and I) and less in the S phase (Fig. 6H and J) following miR-503-3p or miR-503-5p knockdown. In addition, western blotting results showed that

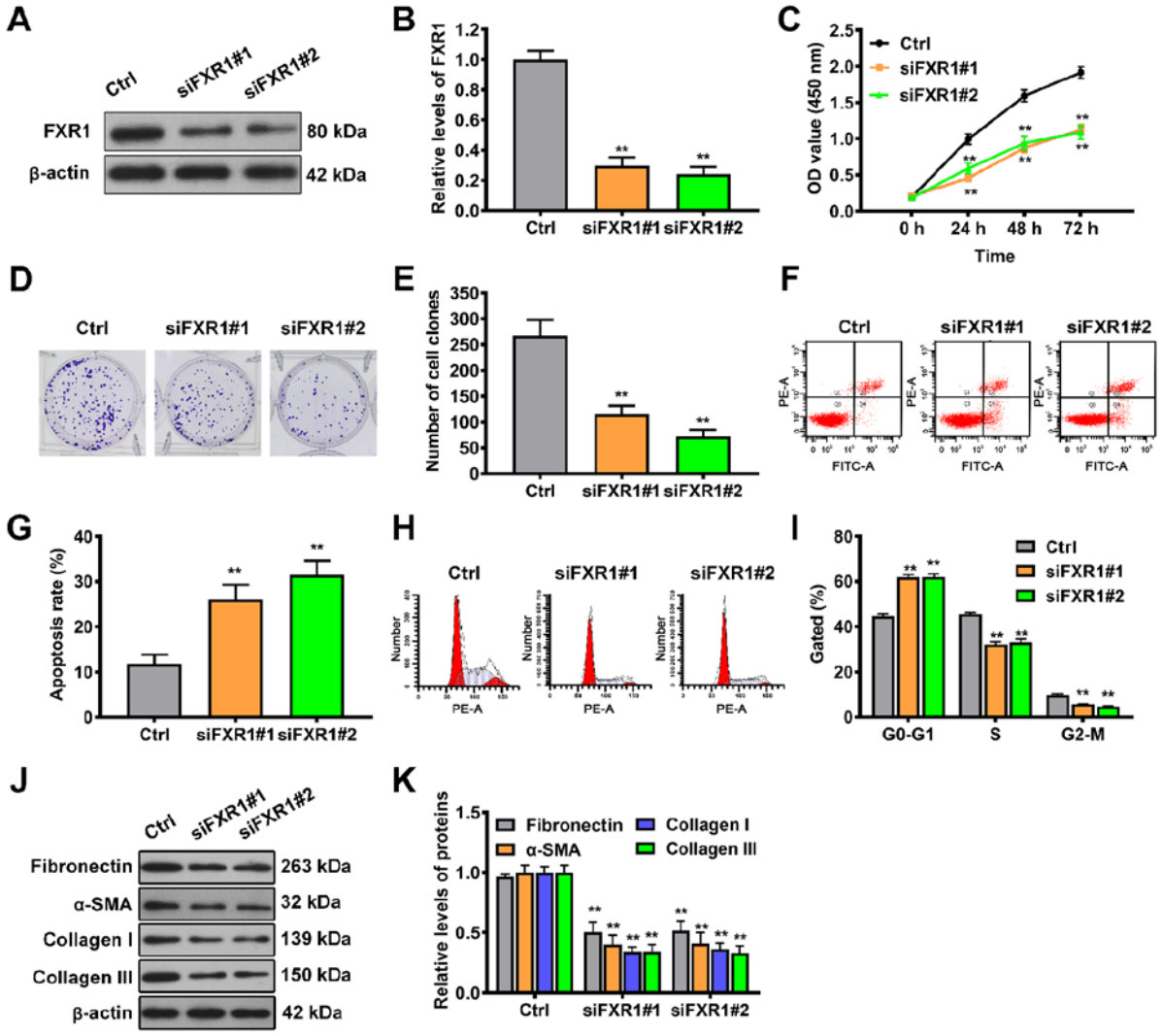

Figure 4. FXR1 promotes keloid-derived fibroblast proliferation and accumulation of extracellular matrix but inhibits apoptosis. (A and B) Knockdown efficiency of FXR1 was investigated in keloid-derived fibroblasts via western blot analysis. (C) Viability of keloid-derived fibroblasts in the presence or absence of FXR1 knockdown was detected by Cell Counting Kit-8 assay. (D and E) Proliferation of keloid-derived fibroblasts was determined by colony formation assay. (F and G) Cell apoptosis and (H and I) cell cycle analysis were determined via flow cytometric assays in siFXR1-transfected keloid-derived fibroblasts. (J and K) Expression levels of extracellular matrix-associated proteins were determined in siFXR1-transfected keloid-derived fibroblasts by western blot assay. **P<0.01 vs. Ctrl. FXR1, Fbxo4-mediated FMR1 autosomal homolog 1; si, small interfering; Ctrl, control; OD, optical density; SMA, smooth muscle actin.

downregulation of miR-503-3p significantly decreased the expression levels of fibronectin, α-SMA, collagen I and III, indicating that extracellular matrix accumulation was reduced (Fig. 6K and L). Consistent with the miR-503-3p results, knockdown of miR-503-5p also led to a significant decrease in the expression levels of fibronectin, α-SMA, collagen I and III (Fig. 6M and N). These results indicated that both miR-503-3p and miR-503-5p contributed to keloid progression.

Discussion

To the best of our knowledge, the present study is the first analysis of circNRIP1-guided keloid progression. circNRIP1 was markedly upregulated in keloid tissue and keloid-derived fibroblasts. Loss-of-function of circNRIP1 promoted cell apoptosis and inhibited proliferation and extracellular matrix accumulation of keloid-derived fibroblasts. Mechanistic studies confirmed that circNRIP1 exerted its keloid-promoting effects via upregulation of FXR1 expression by interacting with FXR1 and protecting it from Fbxo4-mediated ubiquitination and degradation. Consistent with the circNRIP1 results, FXR1 deficiency exhibited similar effects on keloid progression. FXR1 interaction was required for the maturation of pre-miR-503, a precursor of both miR-503-3p and miR-503-5p. Additionally, miR-503-3p and miR-503-5p also facilitated keloid progression. These results provided mechanistic and functional insights into keloid progression and suggested that circNRIP1 may be a novel therapeutic target for keloid treatment (Fig. 7).

The discovery of circRNAs altered understanding of the complex biology of keloids (26-28). Increasing evidence has indicated that dysregulated circRNA expression affects a multitude of cellular processes, including cell proliferation, apoptosis and migration (29,30). For example, Zhang *et al* (28) analyzed the expression profiles of circRNAs and found that 411 were differentially expressed in keloid dermal fibroblasts, 206 of which were upregulated and 205 downregulated. Additionally, overexpression of

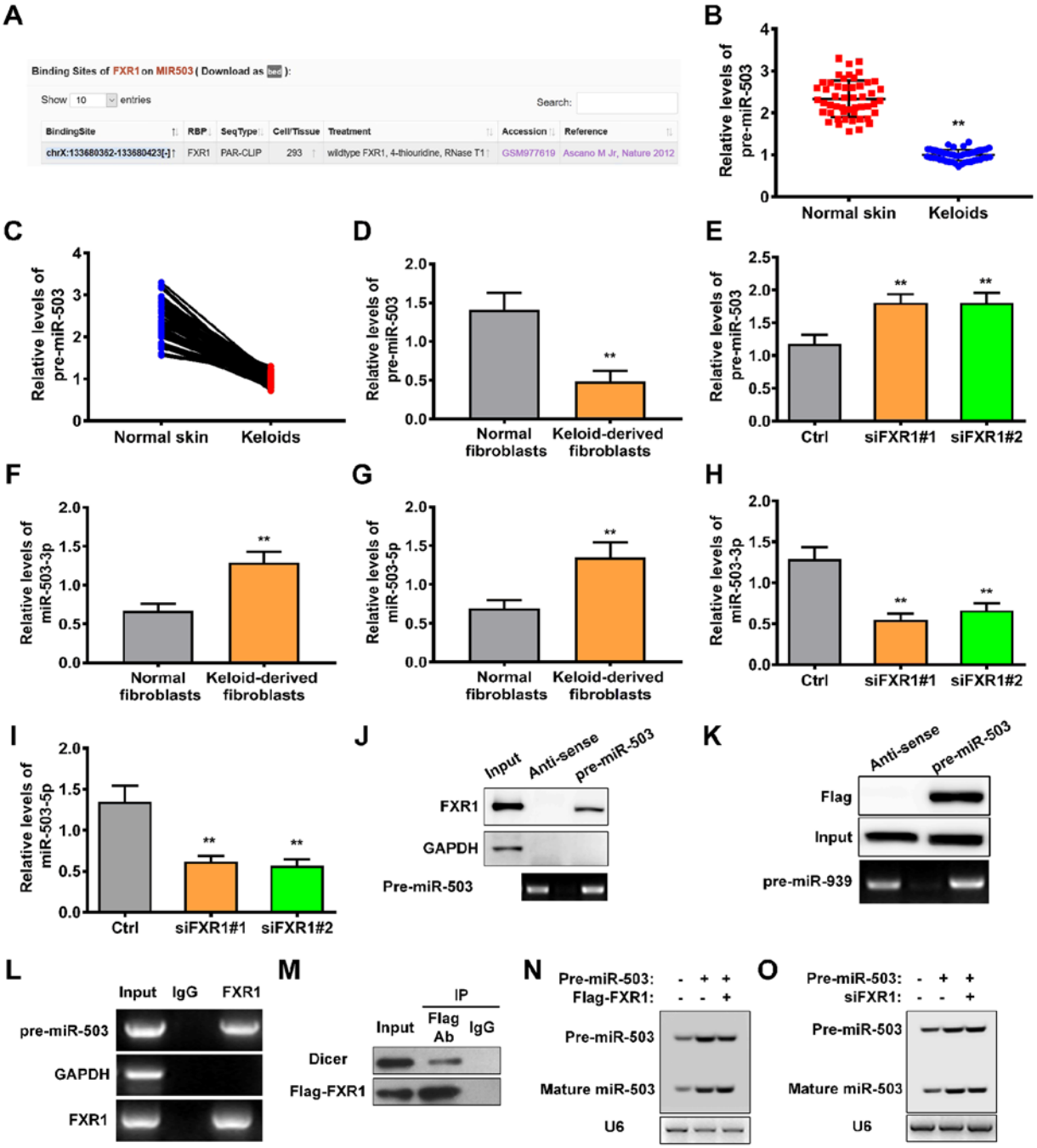

Figure 5. FXR1 promotes the maturation of pre-miR-503 in keloid-derived fibroblasts. (A) Bioinformatics-based (starBase) prediction of FXR1 binding sites on pre-miR-503. (B) Pre-miR-503 levels in keloid and adjacent normal skin tissue were measured by RT-qPCR. (C) Association between pre-miR-503 levels in keloid and adjacent normal skin tissue was determined. (D and E) Pre-miR-503 levels in normal human fibroblasts and keloid-derived fibroblasts in the presence or absence of FXR1 knockdown was evaluated by RT-qPCR. (F and G) miR-503-3p and miR-503-5p levels in normal human fibroblasts and keloid-derived fibroblasts. (H and I) miR-503-3p and miR-503-5p levels in keloid-derived fibroblasts in the presence or absence of FXR1 knockdown was detected by RT-qPCR. (J) Keloid-derived fibroblast lysate was prepared for RNA pulldown with biotinylated pre-miR-503 or antisense transcripts and western blotting analysis was performed using anti-FXR1. GAPDH was used as a control. (K) Interaction between pre-miR-503 and FXR1 was investigated by immunoprecipitation of pre-miR-503 using whole-cell lysate of 293T cells, followed by immunoblotting for FXR1. (L) RNA immunoprecipitation assay was performed using anti-FXR1 or anti-IgG antibodies and pre-miR-503 levels were measured via RT-qPCR; GAPDH and TERC mRNA were used as the negative and positive controls, respectively. (M) Co-immunoprecipitation was performed to investigate the association between Dicer and FXR1 in 293T cells. Northern blot assay was performed to assess the levels of mature miR-503 processed from transfected pre-miR-503 in 293T cells (N) following FXR1 overexpression or (O) in the absence of FXR1. **P<0.01 vs. Ctrl or human normal fibroblasts. FXR1, Fbxo4-mediated FMR1 autosomal homolog 1; miR, microRNA; RT-q, reverse transcription-quantitative; TERC, telomerase RNA component; Ctrl, control; si, small interfering.

hsa_circRNA_0008259 suppressed type I and III collagen expression. circNRIP1, which originates from the *NRIP1* gene, serves a role in cancer progression: circNRIP1 deficiency significantly inhibits the proliferation, migration and invasion abilities of gastric cancer cells (15). These observations suggested that circNRIP1 may be of pathobiological significance in keloid progression. The present study investigated the biological role of circNRIP1 in keloid progression

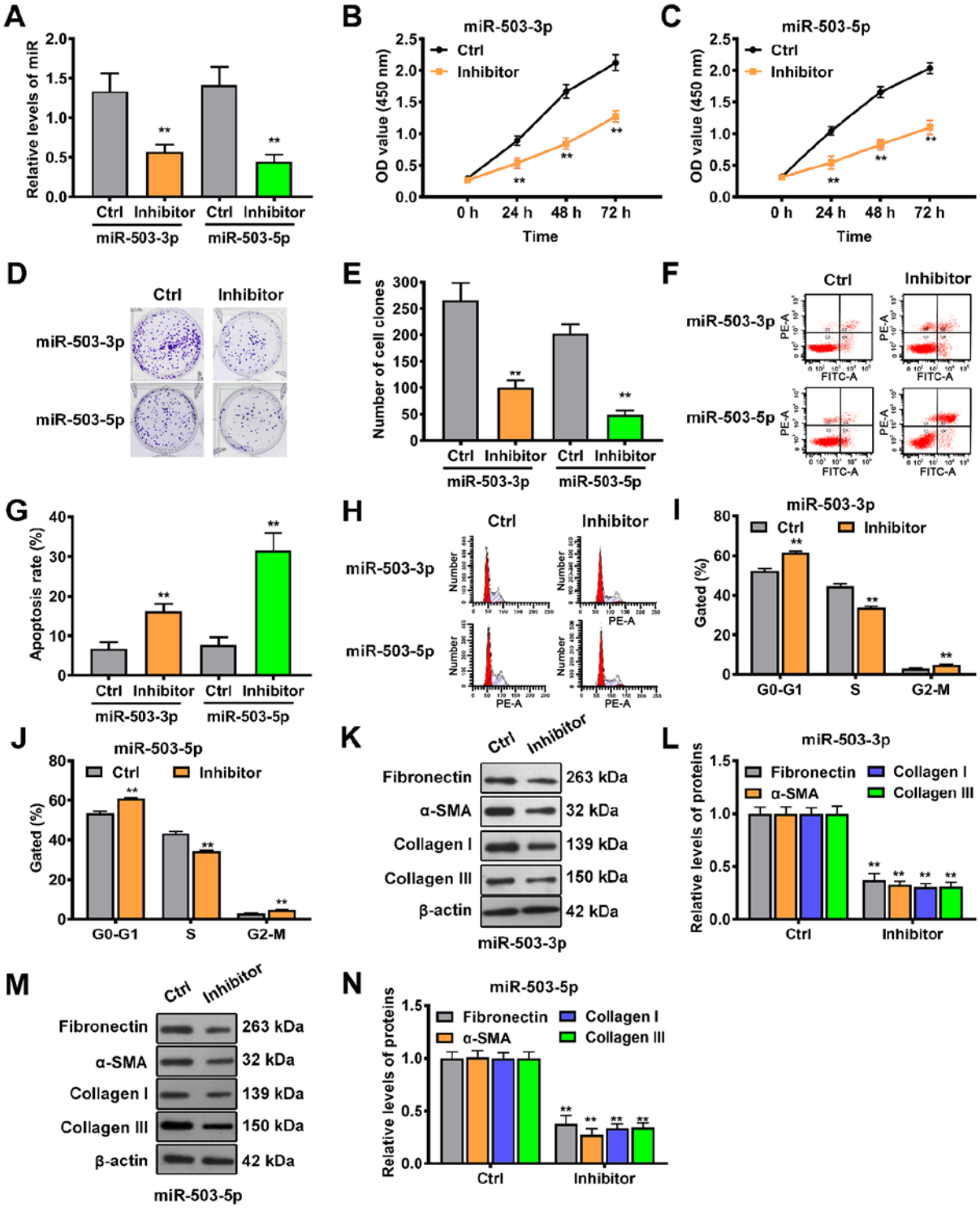

Figure 6. Mature miR-503 induces keloid-derived fibroblast proliferation and accumulation of extracellular matrix but inhibits apoptosis. (A) Knockdown efficiency of the miR-503-3p and miR-503-5p specific inhibitors was investigated in keloid-derived fibroblasts via reverse transcription-quantitative PCR. Viability of keloid-derived fibroblasts transfected with (B) miR-503-3p or (C) miR-503-5p inhibitor was determined by Cell Counting Kit-8 assay. (D and E) Proliferation of miR-503-3p or miR-503-5p inhibitor-transfected keloid-derived fibroblasts was measured by colony formation assay. (F and G) Apoptosis and (H) cell cycle progression in keloid-derived fibroblasts transfected with (I) miR-503-3p or (J) miR-503-5p inhibitor was assessed by flow cytometry. Western blot assays were used to determine the expression levels of extracellular matrix-associated proteins in keloid-derived fibroblasts transfected with (K and L) miR-503-3p or (M and N) miR-503-5p inhibitor. **P<0.01 vs. Ctrl. miR, microRNA; Ctrl, control; OD, optical density; SMA, smooth muscle actin.

and the underlying regulatory mechanisms. To the best of our knowledge, the present study is the first to profile the expression of circNRIP1, which was highly expressed in keloid tissue and keloid-derived fibroblasts. This was consistent with a previous report showing that circNRIP1 is also highly expressed in gastric cancer (15). Although these findings lack clinical evidence, such as an association between circNRIP1 levels and clinicopathological characteristics, they

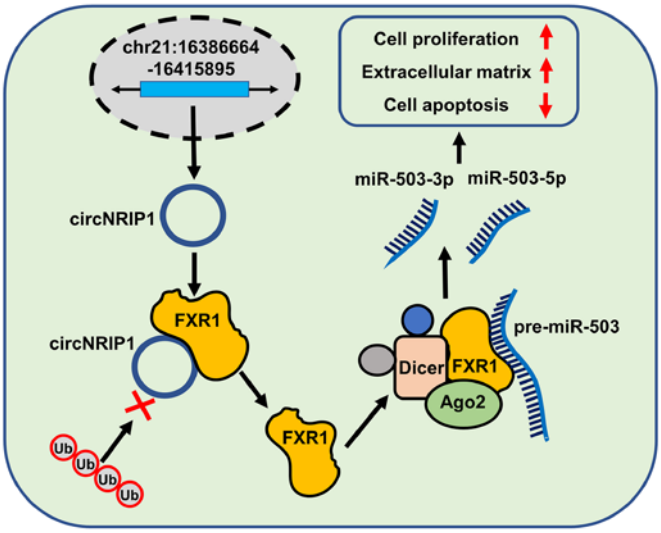

Figure 7. Schematic representation of the mechanism by which circNRIP1 promotes keloid progression. circNRIP1 induced pre-miR-503 maturation via protecting FXR1 from Fbxo4-mediated ubiquitination and degradation, which facilitated proliferation and extracellular matrix accumulation, but inhibited apoptosis, in keloid-derived fibroblasts. circNRIP1, circular nuclear receptor interacting protein 1; miR, microRNA; FXR1, Fbxo4-mediated FMR1 autosomal homolog 1; AGO2, argonaute RISC catalytic component 2.

nevertheless suggested that circNRIP1 may be involved in keloid progression.

Keloids are pathological scars characterized by excessive proliferation and invasive growth of dermal fibroblasts and abnormal deposition of collagen fibers, and exhibit cancer-like properties (31,32). For example, Jin *et al* (33) found abnormal arrangement and hyperplasia of fibers in keloid tissue, along with increased ColI levels. The mechanisms underlying keloid progression are poorly understood and effective prevention and treatment are lacking. To the best of our knowledge, no study has investigated the biological role of circNRIP1 either in keloids or in other types of pathological scar. Loss-of-function analysis here demonstrated that knockdown of circNRIP1 impaired cell proliferation and accumulation of extracellular matrix, and induced cell apoptosis in keloid-derived fibroblasts. To the best of our knowledge, the present study is the first report on the role of circNRIP1 in keloid progression, and the results indicate that silencing circNRIP1 may represent a promising therapeutic strategy for the treatment of keloids. However, *in vivo* experiments are required to confirm the function of circNRIP1 in keloid progression.

Increasing evidence has shown that RNA-binding proteins act in concert with circRNAs in disease progression (34,35). For example, circADD3 has been shown to facilitate enhancer of zeste 2 polycomb repressive complex 2 subunit degradation via CDK1-mediated ubiquitination (36). The present study predicted the downstream targets of circNRIP1 using RNAInter and found that FXR1 interacted with circNRIP1. Several studies have demonstrated that upregulation of FXR1 promotes cell proliferation, migration and invasion (37), which suggested that FXR1 may play a crucial role in keloid progression. Validation experiments confirmed that circNRIP1 maintained FXR1 stability via direct interaction. Accumulating evidence has shown that circRNAs directly bind to RNA-binding proteins and regulate their expression or activity at the post-translational level (38,39). For example, Qie *et al* (40) reported that the E3 ubiquitin ligase Fbxo4 interacts with, and promotes the ubiquitination and degradation of, FXR1. Consequently, it was speculated that circNRIP1 may inhibit FXR1 ubiquitination by blocking the interaction between FXR1 and Fbxo4 in keloid tissue. RNA pulldown and RIP assays verified that circNRIP1 blocked the Fbxo4-mediated ubiquitination of FXR1. Several studies have shown that FXR1 facilitates the malignant behavior of cancer cells (41-43). Inhibition of FXR1 selectively blocks proliferation in human cancer cells (42). Here, *in vitro* loss-of-function experiments demonstrated that FXR1 deficiency markedly decreased cell proliferation and extracellular matrix accumulation but induced cell apoptosis in keloid-derived fibroblasts, further confirming the aforementioned hypothesis. To the best of our knowledge, the present study is the first to demonstrate that circNRIP1 promotes keloid progression via stabilizing FXR1.

Although FXR1 is not the primary regulatory molecule in pre-miRNA processing, studies have shown that FXR1 is involved in the efficient processing of pre-miRNA and forms a complex with pre-miRNA, Dicer and argonaute RISC catalytic component 2 (44,45). Additionally, Majumder and Palanisamy (43) proposed that FXR1 controls the expression of a subset of mature miRNAs, including miR-301a-3p, which is highly expressed in oral cancer cells. In the present study, prediction results obtained from the starBase database indicated that FXR1 interacted with pre-miR-503. Zhong *et al* (46) performed miRNA expression profile analysis and found that both miR-503-3p and miR-503-5p are highly expressed in keloids. Therefore, the present study aimed to characterize the mechanisms underlying FXR1-mediated regulation of pre-miR-503 maturation. Expression profiling showed that the levels of both miR-503-3p and miR-503-5p were significantly upregulated in keloid tissue. However, pre-miR-503 showed the opposite expression profile. These results were consistent with those of Zhong *et al* (46) for microarray data. Moreover, the present findings provided evidence that FXR1 directly interacts with pre-miR-503. FXR1 overexpression led to an increase in the levels of mature miR-503 and a decrease in those of pre-miR-503 *in vitro*. These data highlight a novel molecular mechanism for FXR1 in keloid progression. At present, the roles of miR-503-3p and miR-503-5p in regulating cell proliferation, apoptosis and extracellular matrix accumulation remain contradictory (47,48). Here, knockdown of miR-503-3p or miR-503-5p impaired cell proliferation and excessive extracellular matrix accumulation and promoted cell apoptosis. Consistent with these findings, inhibition of miR-503-5p is reported to suppress chondrocyte proliferation (49), while miR-503-3p enhances the proliferation of breast cancer cells (47). These findings further confirmed the hypothesis that circNRIP1 facilitates keloid progression via FXR1-mediated pre-miR-503 maturation. However, contradictory results have been reported for the roles of miR-503-3p and miR-503-5p in cell proliferation and apoptosis (50,51). For example, Sun *et al* (52) found that miR-503-3p suppresses viability and promotes apoptosis of lung cancer cells. Fu *et al* (50) showed that increasing miR-503-5p expression markedly inhibited the proliferation and colony-forming ability of cervical cancer cells. These discrepancies may be due to different

experimental conditions, such as the use of different cell types. Further studies are needed to confirm the role of miR-503-3p and miR-503-5p in keloids. Additionally, the combination of miR-503-3p and miR-503-5p, as well as their downstream targets need to be further studied in the future.

In conclusion, the present study is the first to show that circNRIP1 is highly expressed in keloid tissue, which triggers cell proliferation and accumulation of extracellular matrix, but inhibits cell apoptosis. Mechanistically, circNRIP1 contributes to pre-miR-503 maturation by antagonizing Fbxo4-mediated FXR1 ubiquitination and degradation. These results provide a novel theoretical and experimental basis for keloid pathogenesis and identify potential therapeutic targets for the treatment of keloids.

Acknowledgements

Not applicable.

Funding

No funding was received.

Availability of data and materials

The datasets generated and/or analyzed during the current study are available from the corresponding author on reasonable request.

Authors' contributions

TW and HY conceptualized the study. BW designed the methodology and collected the data. HZ operated the software and visualized the data. BW validated the data and drafted the manuscript. HZ and TW analyzed the data. HY performed the experiments and supervised the study. TW acquired resources and funding, reviewed and edited the manuscript and was responsible for project administration. All authors read and approved the final version of the manuscript.

Ethics approval and consent to participate

The present study was approved by the Clinical Research Ethics Committee of Zaozhuang Municipal Hospital (approval no. 2018ZMHE015). Additionally, written informed consent was obtained from all patients.

Patient consent for publication

Not applicable.

Competing interests

The authors declare that they have no competing interests.

References

1. Liu T, Ma X, Ouyang T, Chen H, Xiao Y, Huang Y, Liu J and Xu M: Efficacy of 5-aminolevulinic acid-based photodynamic therapy against keloid compromised by downregulation of SIRT1-SIRT3-SOD2-mROS dependent autophagy pathway. Redox Biol 20: 195-203, 2019.
2. Shi K, Qiu X, Zheng W, Yan D and Peng W: MiR-203 regulates keloid fibroblast proliferation, invasion, and extracellular matrix expression by targeting EGR1 and FGF2. Biomed Pharmacother 108: 1282-1288, 2018.
3. Har-Shai Y, Brown W, Labbé D, Dompmartin A, Goldine I, Gil T, Mettanes I and Pallua N: Intralesional cryosurgery for the treatment of hypertrophic scars and keloids following aesthetic surgery: The results of a prospective observational study. Int J Low Extrem Wounds 7: 169-175, 2008.
4. Berman B, Maderal A and Raphael B: Keloids and hypertrophic scars: Pathophysiology, classification, and treatment. Dermatol Surg 43 (Suppl 1): S3-S18, 2017.
5. Yang JY and Yang SY: Are auricular keloids and persistent hypertrophic scars resectable? The role of intrascar excision. Ann Plast Surg 69: 637-642, 2012.
6. Shin JY, Yun SK, Roh SG, Lee NH and Yang KM: Efficacy of 2 representative topical agents to prevent keloid recurrence after surgical excision. J Oral Maxillofac Surg 75: 401.e1-401.e6, 2017.
7. Nong Q, Li S, Wu Y and Liu D: LncRNA COL1A2-AS1 inhibits the scar fibroblasts proliferation via regulating miR-21/Smad7 pathway. Biochem Biophys Res Commun 495: 319-324, 2018.
8. Yan L, Wang LZ, Xiao R, Cao R, Pan B, Lv XY, Jiao H, Zhuang Q, Sun XJ and Liu YB: Inhibition of microRNA-21-5p reduces keloid fibroblast autophagy and migration by targeting PTEN after electron beam irradiation. Lab Invest 100: 387-399, 2020.
9. Zhang G, Guan Q, Chen G, Qian F and Liang J: DNA methylation of the CDC2L1 gene promoter region decreases the expression of the CDK11p58 protein and reduces apoptosis in keloid fibroblasts. Arch Dermatol Res 310: 107-115, 2018.
10. Kristensen LS, Andersen MS, Stagsted LVW, Ebbesen KK, Hansen TB and Kjems J: The biogenesis, biology and characterization of circular RNAs. Nat Rev Genet 20: 675-691, 2019.
11. Yu J, Xu QG, Wang ZG, Yang Y, Zhang L, Ma JZ, Sun SH, Yang F and Zhou WP: Circular RNA cSMARCA5 inhibits growth and metastasis in hepatocellular carcinoma. J Hepatol 68: 1214-1227, 2018.
12. Yao J, Zhang C, Chen Y and Gao S: Downregulation of circular RNA circ-LDLRAD3 suppresses pancreatic cancer progression through miR-137-3p/PTN axis. Life Sci 239: 116871, 2019.
13. Peng Y, Song X, Zheng Y, Cheng H and Lai W: circCOL3A1-859267 regulates type I collagen expression by sponging miR-29c in human dermal fibroblasts. Eur J Dermatol 28: 613-620, 2018.
14. Shi J, Yao S, Chen P, Yang Y, Qian M, Han Y, Wang N, Zhao Y, He Y, Lyu L and Lu D: The integrative regulatory network of circRNA and microRNA in keloid scarring. Mol Biol Rep 47: 201-209, 2020.
15. Zhang X, Wang S, Wang H, Cao J, Huang X, Chen Z, Xu P, Sun G, Xu J, Lv J and Xu Z: Circular RNA circNRIP1 acts as a microRNA-149-5p sponge to promote gastric cancer progression via the AKT1/mTOR pathway. Mol Cancer 18: 20, 2019.
16. Li M, Cai J, Han X and Ren Y: Downregulation of circNRIP1 suppresses the paclitaxel resistance of ovarian cancer via regulating the miR-211-5p/HOXC8 axis. Cancer Manag Res 12: 9159-9171, 2020.
17. Xu G, Li M, Wu J, Qin C, Tao Y and He H: Circular RNA circNRIP1 sponges microRNA-138-5p to maintain hypoxia-induced resistance to 5-fluorouracil through HIF-1α-dependent glucose metabolism in gastric carcinoma. Cancer Manag Res 12: 2789-2802, 2020.
18. Xie R, Tang J, Zhu X and Jiang H: Silencing of hsa_circ_0004771 inhibits proliferation and induces apoptosis in breast cancer through activation of miR-653 by targeting ZEB2 signaling pathway. Biosci Rep: May 17, 2019 (Epub ahead of print). doi: 10.1042/BSR20181919.
19. Wang L, Tong X, Zhou Z, Wang S, Lei Z, Zhang T, Liu Z, Zeng Y, Li C, Zhao J, *et al*: Circular RNA hsa_circ_0008305 (circPTK2) inhibits TGF-β-induced epithelial-mesenchymal transition and metastasis by controlling TIF1γ in non-small cell lung cancer. Mol Cancer 17: 140, 2018.
20. Zheng X, Chen L, Zhou Y, Wang Q, Zheng Z, Xu B, Wu C, Zhou Q, Hu W, Wu C and Jiang J: A novel protein encoded by a circular RNA circPPP1R12A promotes tumor pathogenesis and metastasis of colon cancer via Hippo-YAP signaling. Mol Cancer 18: 47, 2019.
21. Huang X, He M, Huang S, Lin R, Zhan M, Yang D, Shen H, Xu S, Cheng W, Yu J, *et al*: Circular RNA circERBB2 promotes gallbladder cancer progression by regulating PA2G4-dependent rDNA transcription. Mol Cancer 18: 166, 2019.

22. Du WW, Fang L, Yang W, Wu N, Awan FM, Yang Z and Yang BB: Induction of tumor apoptosis through a circular RNA enhancing Foxo3 activity. Cell Death Differ 24: 357-370, 2017.
23. Liang WC, Wong CW, Liang PP, Shi M, Cao Y, Rao ST, Tsui SK, Waye MM, Zhang Q, Fu WM and Zhang JF: Translation of the circular RNA circβ-catenin promotes liver cancer cell growth through activation of the Wnt pathway. Genome Biol 20: 84, 2019.
24. Livak KJ and Schmittgen TD: Analysis of relative gene expression data using real-time quantitative PCR and the 2(-Delta Delta C(T)) method. Methods 25: 402-408, 2001.
25. Hartmann P, Zhou Z, Natarelli L, Wei Y, Nazari-Jahantigh M, Zhu M, Grommes J, Steffens S, Weber C and Schober A: Endothelial Dicer promotes atherosclerosis and vascular inflammation by miRNA-103-mediated suppression of KLF4. Nat Commun 7: 10521, 2016.
26. Patop IL, Wüst S and Kadener S: Past, present, and future of circRNAs. EMBO J 38: e100836, 2019.
27. Wu H, Wu S, Zhu Y, Ye M, Shen J, Liu Y, Zhang Y and Bu S: Hsa_circRNA_0054633 is highly expressed in gestational diabetes mellitus and closely related to glycosylation index. Clin Epigenetics 11: 22, 2019.
28. Zhang Z, Yu K, Liu O, Xiong Y, Yang X, Wang S, Zhang S, Feng Y and Peng Y: Expression profile and bioinformatics analyses of circular RNAs in keloid and normal dermal fibroblasts. Exp Cell Res 388: 111799, 2020.
29. Yu J, Yang M, Zhou B, Luo J, Zhang Z, Zhang W and Yan Z: CircRNA-104718 acts as competing endogenous RNA and promotes hepatocellular carcinoma progression through microRNA-218-5p/TXNDC5 signaling pathway. Clin Sci (Lond) 133: 1487-1503, 2019.
30. Chen X, Ouyang Z, Shen Y, Liu B, Zhang Q, Wan L, Yin Z, Zhu W, Li S and Peng D: CircRNA_28313/miR-195a/CSF1 axis modulates osteoclast differentiation to affect OVX-induced bone absorption in mice. RNA Biol 16: 1249-1262, 2019.
31. Liu J, Ren J, Su L, Cheng S, Zhou J, Ye X, Dong Y, Sun S, Qi F, Liu Z, *et al*: Human adipose tissue-derived stem cells inhibit the activity of keloid fibroblasts and fibrosis in a keloid model by paracrine signaling. Burns 44: 370-385, 2018.
32. Andrews JP, Marttala J, Macarak E, Rosenbloom J and Uitto J: Keloids: The paradigm of skin fibrosis-pathomechanisms and treatment. Matrix Biol 51: 37-46, 2016.
33. Jin J, Zhai HF, Jia ZH and Luo XH: Long non-coding RNA HOXA11-AS induces type I collagen synthesis to stimulate keloid formation via sponging miR-124-3p and activation of Smad5 signaling. Am J Physiol Cell Physiol 317: C1001-C1010, 2019.
34. Dong W, Dai ZH, Liu FC, Guo XG, Ge CM, Ding J, Liu H and Yang F: The RNA-binding protein RBM3 promotes cell proliferation in hepatocellular carcinoma by regulating circular RNA SCD-circRNA 2 production. EBioMedicine 45: 155-167, 2019.
35. Wang L, Long H, Zheng Q, Bo X, Xiao X and Li B: Circular RNA circRHOT1 promotes hepatocellular carcinoma progression by initiation of NR2F6 expression. Mol Cancer 18: 119, 2019.
36. Sun S, Wang W, Luo X, Li Y, Liu B, Li X, Zhang B, Han S and Li X: Circular RNA circ-ADD3 inhibits hepatocellular carcinoma metastasis through facilitating EZH2 degradation via CDK1-mediated ubiquitination. Am J Cancer Res 9: 1695-1707, 2019.
37. Cao S, Zheng J, Liu X, Liu Y, Ruan X, Ma J, Liu L, Wang D, Yang C, Cai H, *et al*: FXR1 promotes the malignant biological behavior of glioma cells via stabilizing MIR17HG. J Exp Clin Cancer Res 38: 37, 2019.
38. Huang S, Li X, Zheng H, Si X, Li B, Wei G, Li C, Chen Y, Chen Y, Liao W, *et al*: Loss of super-enhancer-regulated circRNA Nfix induces cardiac regeneration after myocardial infarction in adult mice. Circulation 139: 2857-2876, 2019.
39. Zang J, Lu D and Xu A: The interaction of circRNAs and RNA binding proteins: An important part of circRNA maintenance and function. J Neurosci Res 98: 87-97, 2020.
40. Qie S, Majumder M, Mackiewicz K, Howley BV, Peterson YK, Howe PH, Palanisamy V and Diehl JA: Fbxo4-mediated degradation of Fxr1 suppresses tumorigenesis in head and neck squamous cell carcinoma. Nat Commun 8: 1534, 2017.
41. Fan Y, Yue J, Xiao M, Han-Zhang H, Wang YV, Ma C, Deng Z, Li Y, Yu Y, Wang X, *et al*: FXR1 regulates transcription and is required for growth of human cancer cells with TP53/FXR2 homozygous deletion. Elife 6: e26129, 2017.
42. Cao H, Gao R, Yu C, Chen L and Feng Y: The RNA-binding protein FXR1 modulates prostate cancer progression by regulating FBXO4. Funct Integr Genomics 19: 487-496, 2019.
43. Majumder M and Palanisamy V: RNA binding protein FXR1-miR301a-3p axis contributes to p21WAF1 degradation in oral cancer. PLoS Genet 16: e1008580, 2020.
44. Xu XL, Zong R, Li Z, Biswas MH, Fang Z, Nelson DL and Gao FB: FXR1P but not FMRP regulates the levels of mammalian brain-specific microRNA-9 and microRNA-124. J Neurosci 31: 13705-13709, 2011.
45. Vasudevan S and Steitz JA: AU-rich-element-mediated upregulation of translation by FXR1 and Argonaute 2. Cell 128: 1105-1118, 2007.
46. Zhong L, Bian L, Lyu J, Jin H, Liu Z, Lyu L and Lu D: Identification and integrated analysis of microRNA expression profiles in keloid. J Cosmet Dermatol 17: 917-924, 2018.
47. Zhao Z, Fan X, Jiang L, Xu Z, Xue L, Zhan Q and Song Y: miR-503-3p promotes epithelial-mesenchymal transition in breast cancer by directly targeting SMAD2 and E-cadherin. J Genet Genomics 44: 75-84, 2017.
48. Jiang SP and Li ZR: MiR-503-5p regulates cell epithelial-to-mesenchymal transition, metastasis and prognosis of hepatocellular carcinoma through inhibiting WEE1. Eur Rev Med Pharmacol Sci 23: 2028-2037, 2019.
49. Jee YH, Wang J, Yue S, Jennings M, Clokie SJ, Nilsson O, Lui JC and Baron J: mir-374-5p, mir-379-5p, and mir-503-5p regulate proliferation and hypertrophic differentiation of growth plate chondrocytes in male rats. Endocrinology 159: 1469-1478, 2018.
50. Fu Y, Meng Y, Gu X, Tian S, Hou X and Ji M: miR-503 expression is downregulated in cervical cancer and suppresses tumor growth by targeting AKT2. J Cell Biochem: Jan 29, 2019 (Epub ahead of print). doi: 10.1002/jcb.28099.
51. Cai X, Nie J, Chen L and Yu F: Circ_0000267 promotes gastric cancer progression via sponging MiR-503-5p and regulating HMGA2 expression. Mol Genet Genomic Med 8: e1093, 2020.
52. Sun Y, Li L, Xing S, Pan Y, Shi Y, Zhang L and Shen Q: miR-503-3p induces apoptosis of lung cancer cells by regulating p21 and CDK4 expression. Cancer Biomark 20: 597-608, 2017.